5-30-2018

Pipecolic Acid Confers Systemic Immunity by Regulating Free Radicals

Caixia Wang
Qingdao Agricultural University, China

Ruiying Liu
University of Kentucky, ruiying.liu@uky.edu

Gah-Hyun Lim
FarmHannong, South Korea

Laura de Lorenzo
University of Kentucky, laura.lorenzo@uky.edu

Keshun Yu
University of Kentucky, kyu0@uky.edu

See next page for additional authors

Pipecolic Acid Confers Systemic Immunity by Regulating Free Radicals

Digital Object Identifier (DOI)
https://doi.org/10.1126/sciadv.aar4509

Notes/Citation Information

Published in *Science Advances*, v. 4, no. 5, eaar4509, p. 1-11.

Authors

Caixia Wang, Ruiying Liu, Gah-Hyun Lim, Laura de Lorenzo, Keshun Yu, Kai Zhang, Arthur G. Hunt, Aardra Kachroo, and Pradeep Kachroo

PLANT SCIENCES

Pipecolic acid confers systemic immunity by regulating free radicals

Caixia Wang,[1]* Ruiying Liu,[1] Gah-Hyun Lim,[1†] Laura de Lorenzo,[2] Keshun Yu,[1] Kai Zhang,[1,3] Arthur G. Hunt,[2] Aardra Kachroo,[1] Pradeep Kachroo[1‡]

Pipecolic acid (Pip), a non-proteinaceous product of lysine catabolism, is an important regulator of immunity in plants and humans alike. In plants, Pip accumulates upon pathogen infection and has been associated with systemic acquired resistance (SAR). However, the molecular mechanisms underlying Pip-mediated signaling and its relationship to other known SAR inducers remain unknown. We show that in plants, Pip confers SAR by increasing levels of the free radicals, nitric oxide (NO), and reactive oxygen species (ROS), which act upstream of glycerol-3-phosphate (G3P). Plants defective in NO, ROS, G3P, or salicylic acid (SA) biosynthesis accumulate reduced Pip in their distal uninfected tissues although they contain wild-type–like levels of Pip in their infected leaves. These data indicate that de novo synthesis of Pip in distal tissues is dependent on both SA and G3P and that distal levels of SA and G3P play an important role in SAR. These results also suggest a unique scenario whereby metabolites in a signaling cascade can stimulate each other's biosynthesis depending on their relative levels and their site of action.

INTRODUCTION

Pathogen infection often results in the induction of defense signaling in the local infected tissues, and these can be categorized as pathogen-associated molecular pattern-triggered immunity (PTI) or effector-triggered immunity (ETI). Induction of PTI involves recognition of conserved pathogen-derived molecules termed elicitors by the host-encoded pattern recognition receptors (*1*). Induction of ETI occurs when plant resistance (R) proteins recognize specialized pathogen effectors termed avirulence (avr) factors. Beside local resistance, induction of ETI also activates systemic acquired resistance (SAR), which is associated with transport of signals generated at the local site, resulting in broad-spectrum resistance against related or unrelated pathogens. A number of SAR inducers have been identified, including the chemical signals salicylic acid (SA) (*2*), azelaic acid (C_9 dicarboxylic acid, AzA) (*3*, *4*), glycerol-3-phosphate (G3P) (*4*, *5*), nitric oxide (NO), reactive oxygen species (ROS) (*6*–*8*), and galactolipids (*9*). Recent results have shown that a linear pathway involving NO⇔ROS⇒AzA⇒G3P functions in parallel with SA-derived signaling and that both pathways are essential for induction of SAR (*4*–*6*, *9*, *10*).

G3P levels are regulated by enzymes that are directly or indirectly involved in G3P biosynthesis, as well as those involved in G3P catabolism (*5*, *11*). G3P is synthesized via the glycerol kinase–mediated phosphorylation of glycerol (encoded by *GLI1*) or the G3P dehydrogenase–mediated reduction of dihydroxyacetone phosphate (encoded by *GLY1*). G3P-mediated signaling is dependent on the lipid transfer protein (LTP) DIR1 (defective in induced resistance) and the LTP-like AZI1 [AzA-insensitive (*3*, *4*)]. DIR1 and AZI1 interact with each other, and G3P is required for *DIR1*/*AZI1* transcript stability (*4*, *11*). Conversely, DIR1 and AZI1 are required for avirulent pathogen–inducible G3P accumulation, suggesting that G3P and DIR1 regulate SAR via a feedback loop (*9*).

AzA is a C9 dicarboxylic acid derived from the hydrolysis of C18 fatty acids (FAs) like oleic acid (18:1) and/or its desaturated derivatives, linoleic acid (18:2) and linolenic acid (18:3) present on the galactolipids monogalactosyldiacylglycerol (MGDG) and digalactosyldiacylglycerol (DGDG) (*4*). The biosynthesis of MGDG and DGDG lipids is catalyzed by the plastidal enzymes MGD1 and DGD1, respectively. The C18 FAs 18:1, 18:2, and 18:3 contain a double bond on C9, which, upon cleavage, form a C9 compound that is eventually converted into AzA (*4*). Different ROS function additively to catalyze the oxidation of C18 unsaturated FAs, resulting in the generation of AzA. AzA in turn stimulates the biosynthesis of G3P, and consequently, exogenous AzA is unable to confer SAR on *gly1* and *gli1* mutants that are defective in G3P biosynthesis (*4*).

Pipecolic acid (Pip) (*12*), a non-protein amino acid, has also been associated with SAR. However, direct evidence for its role, based on classical SAR assays, is still lacking for Pip. In plants, Pip accumulates upon pathogen infection in both infected (local) and uninfected (distal) leaves (*12*). The role of Pip in SAR has been largely linked to its ability to induce SA accumulation (*12*). However, the mechanistic details underlying Pip-mediated SAR and its relation to other known chemical signals have not been studied. Pip is derived from lysine catabolism by lysine aminotransferase (LAT). In *Arabidopsis*, LAT is encoded by ALD1, a chloroplastic protein that, when mutated, shuts down pathogen-induced Pip biosynthesis in both local and distal leaves (*12*). However, ALD1 was recently shown to convert lysine to Δ^1-piperideine-2-carboxylic acid, which is then converted to Pip via ornithine cyclodeaminase (encoded by *SARD4*) (*13*, *14*). Pip levels were substantially different in the local leaves of *ald1* and *sard4* plants; while *ald1* plants were defective in Pip accumulation in both local and distal leaves, *sard4* plants were only defective in distal Pip accumulation. Thus, while ALD1 clearly regulates Pip biosynthesis, the precise role of SARD4 in Pip biosynthesis is unclear given that the *sard4* mutation does not abolish Pip biosynthesis in the infected leaves.

Here, we show that Pip is a chemical inducer of SAR and functions primarily upstream of the NO-ROS-AzA-G3P branch of the SAR pathway. Moreover, like *sard4*, plants defective in the biosynthesis

[1]Department of Plant Pathology, University of Kentucky, Lexington, KY 40546, USA. [2]Department of Plant and Soil Sciences, University of Kentucky, Lexington, KY 40546, USA. [3]College of Agronomy and Biotechnology, Southwest University, Chongqing 400716, P.R. China.
*Present address: Qingdao Agricultural University, No. 700, Changcheng Road, Chengyang District, Qingdao City, 266109, P.R. China.
†Present address: FarmHannong 39-23, Dongan-ro 1113beon-gil, Yeonmu-eup, Nonsan-si, Chungcheongnam-do 33010, Korea.
‡Corresponding author. Email: pk62@uky.edu

of ROS, AzA, G3P, or SA are defective in distal but not local Pip accumulation. We propose that the transport of SA and G3P to the distal tissue is important for Pip biosynthesis, where Pip in turn initiates the de novo synthesis of G3P. Together, these data establish the relationship between Pip and other structurally diverse chemical signals associated with SAR and highlight their coordinated function in the induction of SAR.

RESULTS

Exogenous application of Pip confers SAR

An earlier study showed that whole plant application of Pip induces immunity in plants (*12*). To test the requirement for Pip in SAR, we assayed its ability to induce immunity in distal untreated tissue when applied in a localized manner. For this, we pre-infiltrated wild-type (WT) plants (ecotype Col-0) with $MgCl_2$, *Pseudomonas syringae* pv. *tomato* (*Pst avrRpt2*), Pip (1 mM), or methanol (negative control). The distal untreated leaves of all plants were then challenged with a virulent strain of *Pst* (DC3000), and the growth of *Pst* DC3000 was monitored at 0 and 3 days post infiltration (dpi). WT plants previously infected with *Pst avrRpt2* contained ~10- to 15-fold less *Pst* DC3000 compared to $MgCl_2$ pre-infiltrated plants (Fig. 1A). Notably, pre-infiltration of Pip significantly reduced the growth of *Pst* DC3000 (Fig. 1A), indicating that localized application of Pip induced systemic immunity. To confirm this finding, we assayed Pip-mediated SAR in the *ald1* mutant, which is defective in LAT activity and consequently unable to accumulate Pip (Fig. 1B and fig. S1A). Local application of Pip was able to restore SAR in the *ald1* mutant (Fig. 1B), establishing that Pip is required for SAR.

To determine the optimal concentration of Pip required to yield a robust SAR, we applied different concentrations (1 to 2000 μM) of Pip on the local leaf and infected the distal untreated leaves with *Pst* DC3000. SAR was strongest (as detected by a decrease in *Pst* DC3000 proliferation) in plants infiltrated with concentrations of 500 to 1000 μM Pip (Fig. 1C and fig. S1B). However, higher concentrations (2000 μM) of Pip consistently induced significantly weaker

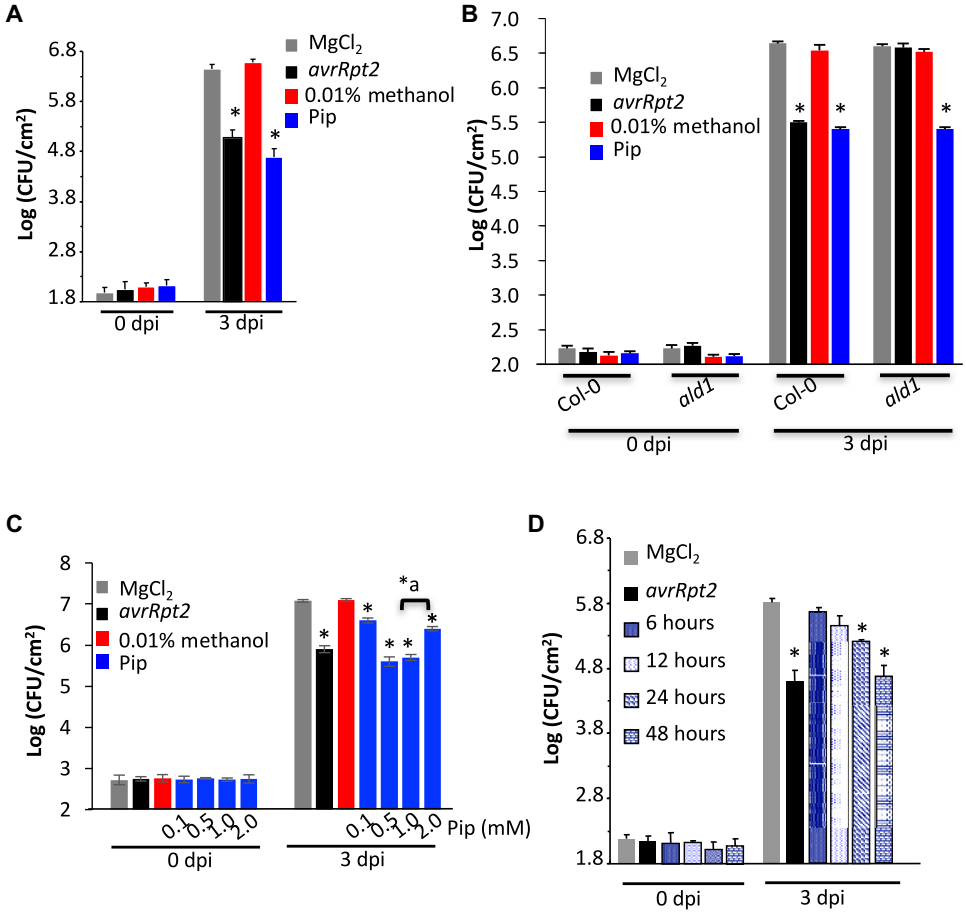

Fig. 1. Pip confers SAR in a dose-dependent manner. (**A**) SAR response in distal leaves of WT Col-0 plants treated locally with $MgCl_2$, methanol (0.01%), avirulent pathogen (*avrRpt2*), or Pip (1000 μM). The virulent pathogen (DC3000) was inoculated 48 hours after local treatments. Error bars indicate SD ($n = 4$). CFU, colony-forming units. (**B**) SAR response in distal leaves of Col-0 and *ald1* plants treated locally with $MgCl_2$, methanol (0.01%), avirulent pathogen (*avrRpt2*), or Pip (1000 μM). The virulent pathogen (DC3000) was inoculated 48 hours after local treatments. Error bars indicate SD ($n = 4$). (**C**) SAR response in distal leaves of WT Col-0 plants treated locally with $MgCl_2$, methanol (0.01%), avirulent pathogen (*avrRpt2*), and different concentrations of Pip (100 to 2000 μM). The virulent pathogen (DC3000) was inoculated 48 hours after local treatments. Error bars indicate SD ($n = 4$). (**D**) SAR response in distal leaves of Col-0 plants treated locally with $MgCl_2$, avirulent pathogen (*avrRpt2*), or Pip (1000 μM each). The virulent pathogen (DC3000) was inoculated at indicated hours after local treatments with Pip. Error bars indicate SD ($n = 4$). For (A) to (D), asterisks and "*a" denote significant differences with mock-treated plants (*t* test, $P < 0.05$) or plants treated with 1 and 2 mM Pip, respectively. The percentage of methanol for control experiments was determined on the basis of dilution prepared from Pip stock solutions. The results are representative of three to five independent experiments.

SAR; SAR induced by 2000 μM Pip was comparable to that induced by 100 μM Pip (Fig. 1C). These data suggested that Pip induced SAR in a concentration-dependent manner and that 500 to 1000 μM Pip was an optimal concentration for the induction of SAR. To determine the time frame of Pip efficacy, SAR was assessed at different times after treatment with 1 mM Pip. WT plants were infiltrated with Pip; their distal leaves were inoculated with *Pst* DC3000 at 6, 12, 24, or 48 hours after Pip infiltration; and *Pst* DC3000 growth was monitored at 0 and 3 dpi. As expected, WT plants previously infected with *Pst avrRpt2* induced SAR compared to plants pre-infiltrated with $MgCl_2$ in their local leaves (Fig. 1D). The 24- and 48-hour time points produced a higher SAR compared to 6 and 12 hours, and the SAR was most effective when virulent pathogen was inoculated 48 hours after Pip application (Fig. 1D).

Pip functions upstream of NO, ROS, AzA, and G3P

To understand the molecular signaling pathway underlying Pip-mediated SAR and its dependence on other SAR-associated signals, we conducted a transcriptome analysis of Pip-treated plants. Col-0 leaves treated with Pip showed an induction of 119 genes, of which 28 genes were shared between Pip- and avr-induced Col-0 plants (Fig. 2A, left). Likewise, 93 of 320 genes down-regulated by Pip were shared between plants treated with Pip and avr (Fig. 2A, right). A survey of genes induced by Pip included several defense-associated genes

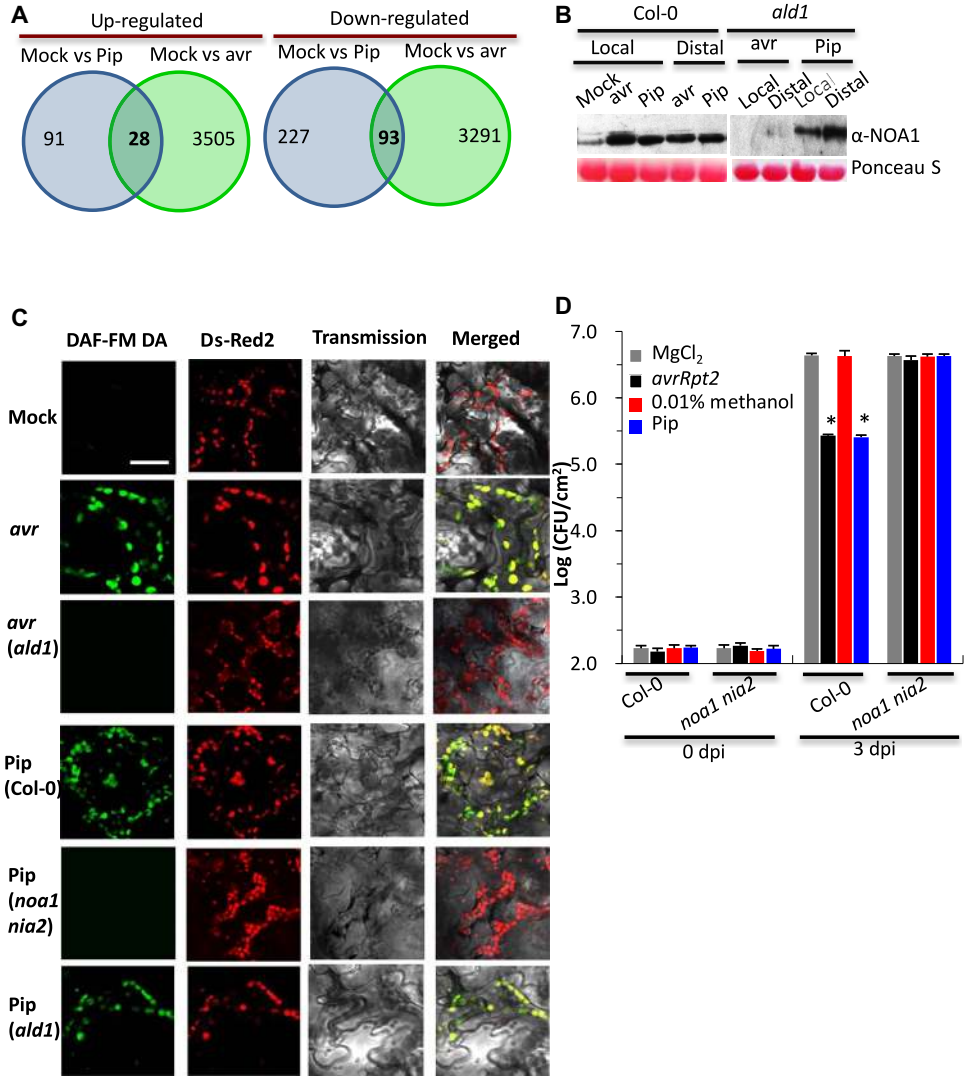

Fig. 2. Pip increases NO levels, and Pip-conferred SAR is dependent on NOA1 NIA proteins. (**A**) Venn diagrams showing the number of genes up-regulated (left) or down-regulated (right) in local tissues of Col-0 plants treated with Pip or water. (**B**) Protein immunoblot showing NOA1 levels in local and distal tissues of Col-0 and *ald1* plants treated with $MgCl_2$ (mock), *avrRpt2* bacteria, or Pip. Leaves were sampled 24 hours after inoculations. Ponceau S staining of the immunoblot was used as the loading control. The experiment was repeated four times with similar results. (**C**) Confocal micrograph showing pathogen-and Pip-induced NO accumulation in Col-0 plants at 24 hours after treatments. The leaves were inoculated with $MgCl_2$ (mock) or *avrRpt2 Pst*, or treated with Pip, and at least 10 independent leaves were analyzed in four experiments with similar results. Chloroplast autofluorescence (red) was visualized using Ds-Red2 channel. Scale bar, 10 μm. DAF-FM DA, 4-amino-5-methylamino-2′,7′-difluorofluorescein diacetate. (**D**) SAR response in distal leaves of Col-0 and *noa1 nia2* plants treated locally with $MgCl_2$, methanol (0.01%), avirulent pathogen (*avrRpt2*), or Pip (1000 μM). The virulent pathogen (DC3000) was inoculated 48 hours after local treatments. Error bars indicate SD ($n = 4$). Asterisks denote significant differences with mock-treated plants (*t* test, $P < 0.05$), and results are representative of three independent experiments.

including *PAD4*, *RBOHD*, *GRX*, and *AtNOA1* (table S1 and fig. S2A). Notably, *PR-1*, which is used as the marker gene for SA, was not induced by Pip (fig. S2A, top) and this in turn was consistent with basal levels of SA in Pip-treated plants (fig. S2B).

Induction of *AtNOA1*, a gene that contributes to NO accumulation after avirulent pathogen infection (*6*), prompted us to analyze NOA1 and NO levels after Pip treatment. Both *avrRpt2* infection and Pip application induced NOA1 protein in local and distal leaves (Fig. 2B). The *avrRpt2* infection was unable to induce NOA1 protein in *ald1* plants, but the *ald1* plants induced WT-like levels of NOA1 after Pip application (Fig. 2B). An induction of NOA1 was associated with increased NO levels primarily in the chloroplasts of *avrRpt2*- or Pip-treated plants (Fig. 2C). As expected, Pip application did not induce NO in *noa1 nia2* plants (Fig. 2C). NIA2 is one of the two isoforms of nitrate reductase, which generates NO from nitrate. A mutation in NOA1 and either NIA1 or NIA2 abolishes avirulent pathogen–induced NO accumulation in *Arabidopsis* (*15*). Notably, consistent with previous results (*6*), the distal leaves of WT plants accumulated less NO compared to local leaves although these tissues accumulated similar levels of NOA1 protein (fig. S2C). Like WT, the *ald1* plants accumulated NO after Pip application but not after *avrRpt2* infection (Fig. 2C and fig. S2D). Together, these results suggested that Pip induces SAR by inducing NO accumulation and that depleted NO levels in *ald1* plants are associated with their inability to accumulate Pip. To confirm that Pip functioned upstream of NO, we assayed Pip-mediated SAR in *noa1 nia2* plants that do not accumulate NO in response to avirulent pathogen (*6*, *15*). Pip was unable to confer SAR on *noa1 nia2* plants (Fig. 2D), thus confirming that Pip-mediated SAR required NO.

Earlier, we showed that ROS, AzA, and G3P operate downstream of NO in the SAR pathway. To test the involvement of these chemical signals in Pip-mediated signaling, we assayed the levels of these metabolites after Pip treatment and Pip-mediated SAR in mutants that are unable to accumulate ROS, AzA, or G3P. Exogenous treatment with Pip resulted in the accumulation of ROS in WT Col-0 plants, and this in turn was associated with increased cell death on Pip-treated leaves (fig. S3A). Pip treatment did not induce ROS accumulation in the *RBOHD* mutant (Fig. 3A and fig. S3, B and D), which is defective in avirulent pathogen–induced ROS biosynthesis (*6*). ROS was measured using both quantitative assays and histochemical staining (Fig. 3A and fig. S3, B to D), and both assays showed similar results. The electron spin resonance (ESR) spectrometry–based quantitative analysis was carried out using α-(4-pyridyl *N*-oxide)-*N*-*tert*-butylnitrone (POBN), which detects hydroxyl and carbon-centered radicals (fig. S3C). A time-course analysis for Pip-induced ROS accumulation showed that ROS levels increased within 6 hours after treatment (fig. S3E). Pip-treated plants did not show microscopic cell death at 6 hours after treatment (fig. S3A), suggesting that Pip-induced ROS accumulation precedes cell death.

Consistent with our results with *noa1 nia2* plants, Pip was unable to confer SAR on *rbohD* or *rbohF* plants, both of which are required for avirulent pathogen–induced ROS accumulation (*16*) and SAR (Fig. 3B) (*6*). As predicted, Pip treatment also increased AzA levels (Fig. 3C) but not in the *rbohD* mutant (fig. S3F). Likewise, Pip treatment increased G3P levels (Fig. 3D), and exogenous Pip was unable to confer SAR on mutants defective in AzA biosynthesis (*mgd1*, *dgd1*, or *mgd1 dgd1* double mutant, data not shown for the single mutant) or G3P (*gly1*, *gli1*, or *gly1 gli1* double mutant) (Fig. 3, E and F). Together, these results suggest that Pip-mediated SAR was dependent on the NO-ROS-AzA-G3P branch of the SAR pathway.

To reconfirm that Pip functions upstream of the NO-ROS-AzA-G3P branch of the SAR pathway, we assayed levels of various SAR-associated chemicals in *ald1* mutant plants, which are compromised in Pip biosynthesis (fig. S1A). We expected *ald1* plants to be compromised in ROS, AzA, and G3P accumulation because our results suggested that Pip functions upstream of NO. Avirulent pathogen–inoculated *ald1* plants failed to accumulate ROS (Fig. 4A and fig. S4A), AzA (Fig. 4B), or G3P (Fig. 4C) but did accumulate WT-like levels of SA (Fig. 4D). Consistent with their inability to accumulate ROS, the *ald1* plants showed reduced ion leakage (fig. S4B), and this phenotype was reminiscent of the reduced ion leakage seen in *rboh* mutants (*16*). The *ald1* plants contained WT-like levels of C18 FAs and galactolipids that serve as precursors for AzA (fig. S4, C and D) (*6*). This suggests that the reduced AzA levels in *ald1* plants were likely due to their inability to accumulate ROS rather than a defect in FAs or galactolipid levels. Consistent with this notion, localized application of ROS, AzA, or G3P was able to restore SAR in *ald1* plants (Fig. 4, E to G), whereas exogenous SA did not (Fig. 4H). Unlike ROS, AzA, and SA, G3P when applied by itself is a poor inducer of SAR because of the presence of phosphatases that can degrade G3P (*5*). Together, these results strongly support a role for Pip upstream of the NO-ROS-AzA-G3P branch of the SAR pathway. This inferred upstream role is further correlated with the fact that Pip was unable to induce SAR in mutants impaired in SA biosynthesis (*sid2*) or signaling (*npr1* and *pad4*) (fig. S5A).

We considered the possibility that Pip serves as a mobile signal during SAR because it functions upstream of NO. We tested whether impaired Pip biosynthesis affected SAR signal generation or perception. For this experiment, we collected petiole exudates (PEXs) from WT (PEX–Col-0) and *ald1* (PEX-*ald1*) plants that were pre-infiltrated with either $MgCl_2$ (PEX_{MgCl2}) or *Pst avrRpt2* (PEX_{avr}). These were then infiltrated into a fresh set of WT and *ald1* plants followed by inoculation of distal leaves with *Pst* DC3000 (Fig. 4I). The growth of *Pst* DC3000 was monitored at 0 and 3 dpi. The PEX_{avr} from *ald1* conferred SAR on Col-0 plants but not on *ald1* plants. Likewise, the PEX_{avr} from Col-0 plants induced SAR on Col-0 but not on *ald1* plants (Fig. 4I). Together, these data suggested that *ald1* plants can generate the SAR signal that functions upstream of Pip. PEX_{avr} from *ald1* plants were able to induce Pip levels in Col-0 plants (fig. S5B). Thus, Pip acts downstream of an unknown SAR signal.

Pip accumulation in distal tissues is dependent on SA and G3P

Quantification of Pip in plants inoculated with avirulent pathogens showed that Pip levels in infected leaves were ~2- to 3-fold higher compared to distal tissue (Fig. 5A). Furthermore, localized application of Pip also increased Pip levels in the distal tissue (Fig. 5A). To test whether Pip was mobile, we first assayed Pip in the distal leaves of Col-0 and *ald1* plants after localized application of Pip. The rationale was that any Pip accumulating in the distal tissue of *ald1* plants would represent Pip that was transported from the treated leaves because this mutant cannot synthesize Pip de novo. Distal leaves of *ald1* plants did accumulate Pip, although these levels were ~15-fold lower as compared to WT plants (fig. S6A). The reduced distal accumulation of Pip in *ald1* plants was unlikely to be related to a defect in transport since localized Pip application rescued the SAR defect in these plants (Fig. 1B). Together, these results suggest that Pip is likely mobile and that transport of Pip to distal tissues is associated with its de novo synthesis. To ascertain this possibility, we extracted Pip from PEX collected from mock-treated (PEX_{mock}) or Pip-treated (PEX_{Pip}) plants. The

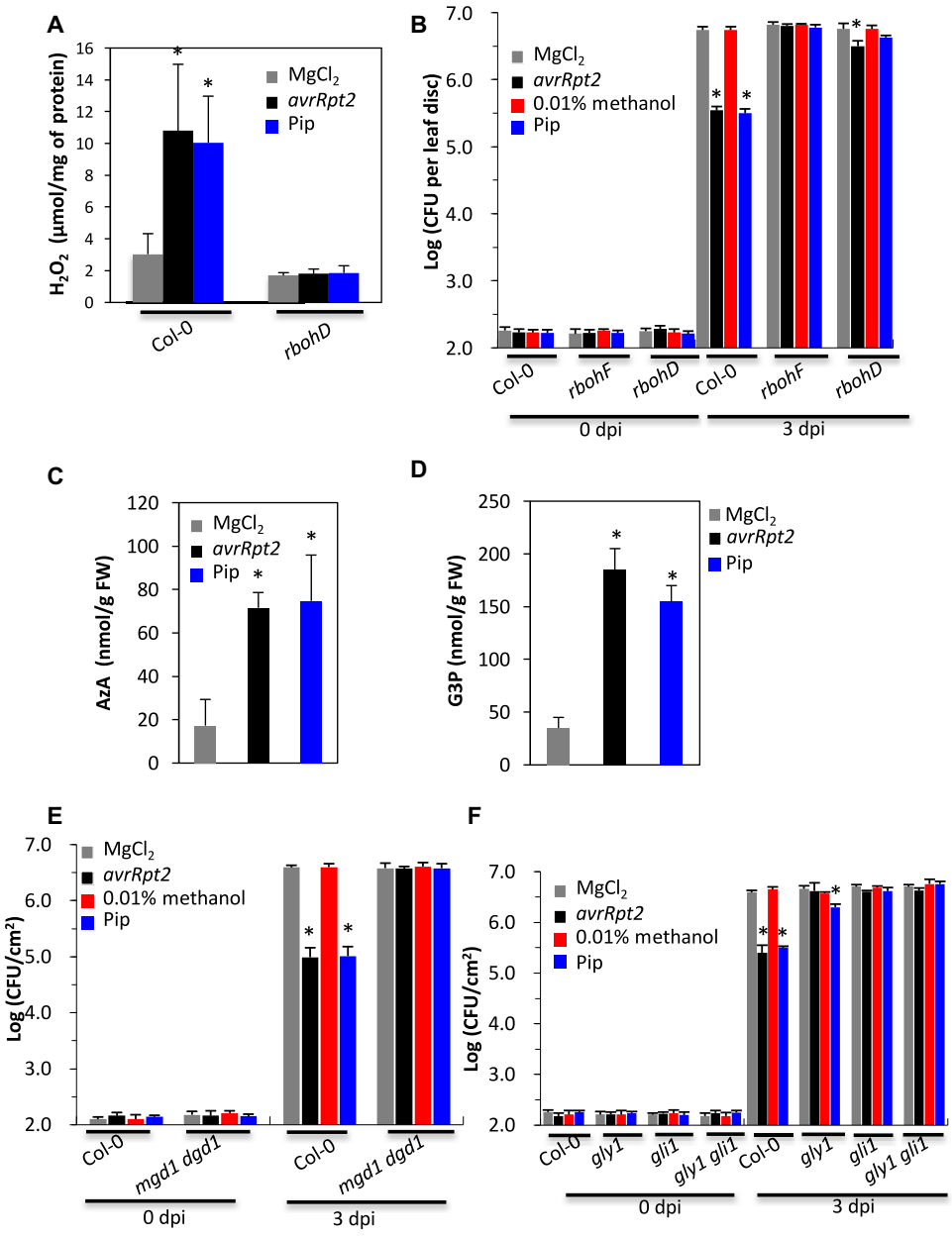

Fig. 3. Pip increases ROS, AzA, and G3P levels, and Pip-mediated SAR is dependent on RBOHD/F, MGD1 DGD1, and GLY1 GLI1 proteins. (**A**) H_2O_2 levels in local tissues after mock and pathogen (*avrRpt2*) inoculations or Pip treatments of Col-0 and *rbohD* plants. The leaves were sampled 24 hours after treatments. The error bars represent SD. H_2O_2 was quantified from the tissue extracts prepared as described in Materials and Methods. Asterisks denote a significant difference with mock (*t* test, $P < 0.05$). The experiment was repeated twice with similar results. (**B**) SAR response in distal leaves of Col-0, *rbohD*, and *rbohF* plants treated locally with $MgCl_2$, methanol (0.01%), avirulent pathogen (*avrRpt2*), or Pip (1000 μM). The virulent pathogen (DC3000) was inoculated 48 hours after local treatments. Error bars indicate SD ($n = 4$). Asterisks denote a significant difference with mock (*t* test, $P < 0.05$). The experiment was repeated four times with similar results for Col-0 and *rbohF* plants. The *rbohD* plants showed a nominal SAR after *avrRpt2* inoculation in two of the four repeats. (**C**) AzA levels in local tissues after mock and pathogen (*avrRpt2*) inoculations or Pip treatments of Col-0 plants. The error bars represent SD. Asterisks denote a significant difference with mock (*t* test, $P < 0.05$). The experiment was repeated three times with similar results. (**D**) G3P levels in local tissues after mock and pathogen (*avrRpt2*) inoculations or Pip treatments of Col-0 plants. The error bars represent SD. Asterisks denote a significant difference with mock (*t* test, $P < 0.05$). The experiment was repeated three times with similar results. (**E**) SAR response in distal leaves of Col-0 and *mgd1 dgd1* plants treated locally with $MgCl_2$, methanol (0.01%), avirulent pathogen (*avrRpt2*), or Pip (1000 μM). The virulent pathogen (DC3000) was inoculated 48 hours after local treatments. Error bars indicate SD ($n = 4$). Asterisks denote a significant difference with mock (*t* test, $P < 0.05$). The experiment was repeated two times with similar results. (**F**) SAR response in distal leaves of Col-0, *gly1*, *gli1*, or *gly1 gli1* plants treated locally with $MgCl_2$, methanol (0.01%), avirulent pathogen (*avrRpt2*), or Pip (1000 μM). The virulent pathogen (DC3000) was inoculated 48 hours after local treatments. Error bars indicate SD ($n = 4$). Asterisks denote a significant difference with mock (*t* test, $P < 0.05$). The experiment was repeated four times with similar results for Col-0, *gli1*, and *gly1 gli1* plants. The *gly1* plants showed a nominal SAR after Pip treatment in two of the four repeats. FW, fresh weight.

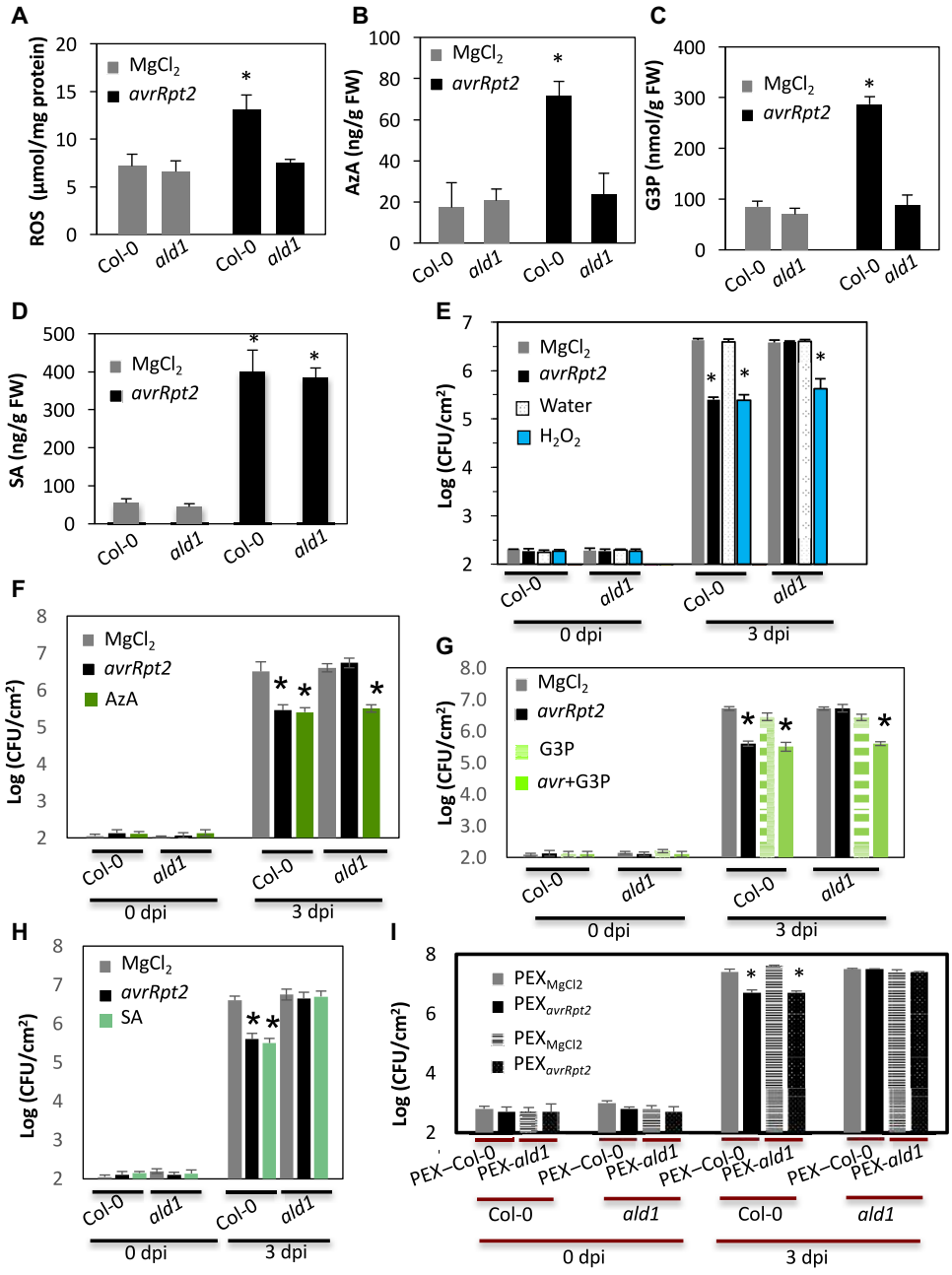

Fig. 4. A defect in Pip biosynthesis in *ald1* plants impairs accumulation of ROS, AzA, and G3P but not SA. (**A** to **D**) H_2O_2 (A), AzA (B), G3P (C), or SA (D) levels in local tissues after mock and pathogen (*avrRpt2*) inoculations of Col-0 and *ald1* plants. The leaves were sampled 24 hours after treatments. The error bars represent SD. Asterisks denote a significant difference with mock (*t* test, $P < 0.05$). The experiment was repeated three times with similar results. (**E** to **H**) SAR response in distal leaves of Col-0 and *ald1* plants treated locally with $MgCl_2$, avirulent pathogen (*avrRpt2*), or H_2O_2 (500 μM; E), AzA (1000 μM; F), G3P (100 μM; G), and SA (500 μM; H). The virulent pathogen (DC3000) was inoculated 48 hours after local treatments. Error bars indicate SD ($n = 4$). Asterisks denote a significant difference with mock (*t* test, $P < 0.05$). The experiment was repeated three times with similar results. (**I**) SAR response in Col-0 and *ald1* plants infiltrated with PEX collected from Col-0 or *ald1* plants that were treated either with $MgCl_2$ (PEX_{MgCl2}) or *avrRpt2* ($PEX_{avrRpt2}$). The distal leaves were inoculated with virulent pathogen at 48 hours after infiltration of primary leaves. Error bars indicate SD ($n = 4$). Asterisks denote a significant difference with mock (*t* test, $P < 0.05$). The experiment was repeated twice with similar results.

PEX_{Pip} accumulated elevated levels of Pip compared to PEX_{mock} (Fig. 5B), suggesting that Pip was indeed mobile. We confirmed this by infiltrating 26 μM ^{14}C-labeled Pip into leaves of WT plants and analyzed Pip extracts by thin-layer chromatography (TLC). The TLC analysis showed a band corresponding to ^{14}C-Pip in both local and distal leaves of mock- and *avrRpt2*-inoculated plants (Fig. 5C). This suggested that bulk of the ^{14}C-Pip was retained and transported as Pip or compounds structurally similar to Pip. The transport assays also showed that *avrRpt2* infection promoted transport of Pip into distal tissues by ~2-fold (Fig. 5C and fig. S6B).

Notably, Pip accumulation in local and distal leaves of Col-0 plants correlated with the induction of *ALD1* expression (fig. S6, C and D),

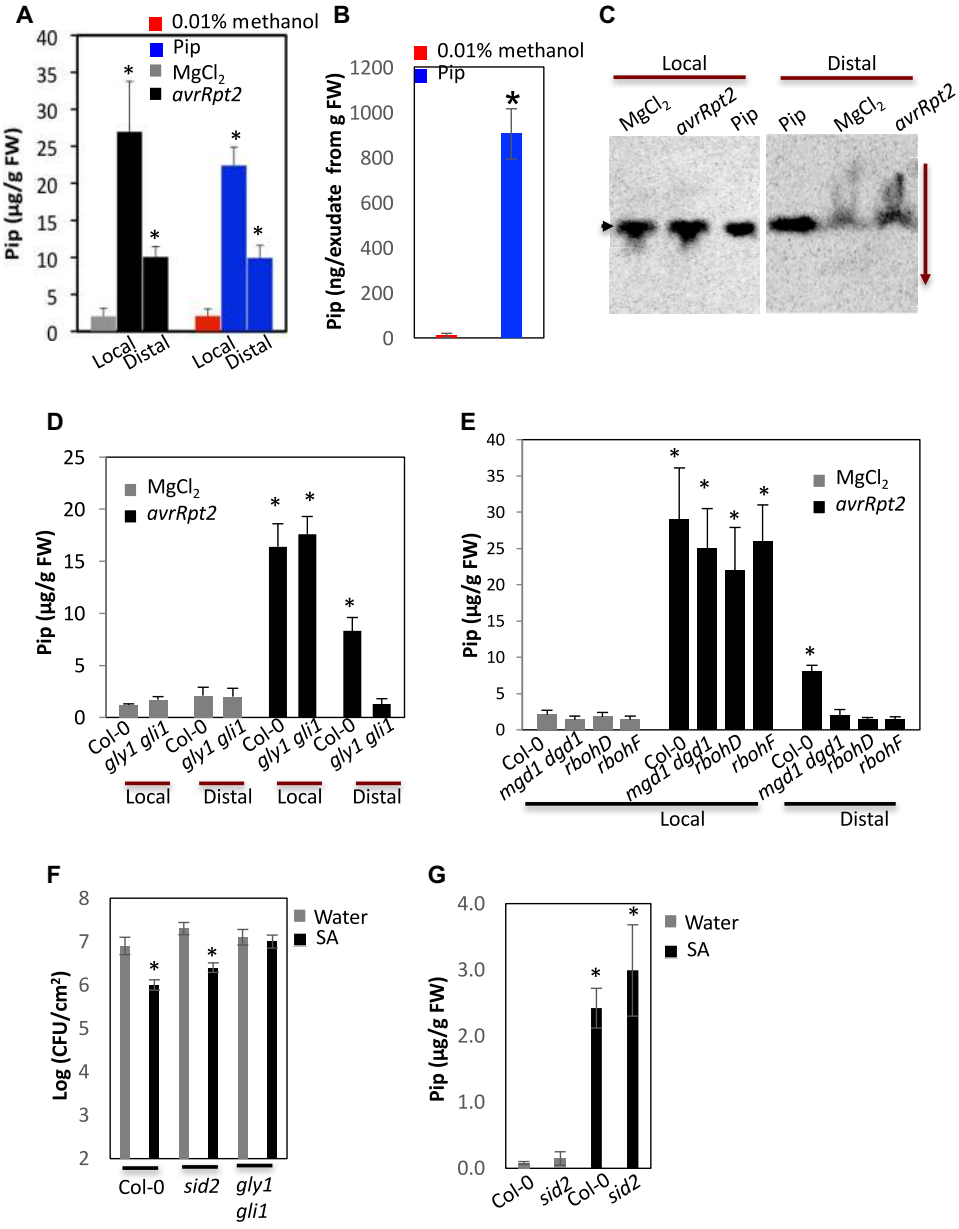

Fig. 5. Induction of Pip in the distal tissues is associated with transport of SA and G3P. (**A**) Pip levels in local and distal tissues of Col-0 plants after mock and pathogen (*avrRpt2*) inoculations or localized application of methanol (0.01%) or Pip. The leaves were sampled 48 hours after treatments. The error bars represent SD. Asterisks denote a significant difference with mock (*t* test, $P < 0.05$). The experiment was repeated three times with similar results. (**B**) Pip levels in PEX collected from Col-0 plants after Pip treatment. The leaves were treated with 1 mM Pip, and the infiltrated leaves (~2 g per sample) were sampled 48 hours after treatment. The error bars represent SD. Asterisks denote a significant difference from mock treatment (*t* test, $P < 0.05$). The experiment was repeated two times with similar results. (**C**) Autoradiograph of TLC plate showing transport of ^{14}C-Pip from the local to distal leaves. ^{14}C-Pip (26 μM) was mixed with $MgCl_2$ (mock) or *avrRpt2* and infiltrated in the local leaves of Col-0 plants. Both local and distal leaves were sampled 24 hours after treatment and analyzed on a silica TLC plate using a butanol/acetic acid/water (3:1:1, v/v) solvent system. The arrowhead indicates the position of the ^{14}C-Pip. The vertical arrow indicates the direction of the run. (**D**) Pip levels in local and distal tissues of Col-0 and *gly gli1* plants after mock and pathogen (*avrRpt2*) inoculations. The leaves were sampled 48 hours after treatments. The error bars represent SD. Asterisks denote a significant difference from mock treatment (*t* test, $P < 0.05$). The experiment was repeated two times with similar results. (**E**) Pip levels in local and distal tissues of Col-0, *mgd1 dgd1*, *rbohD*, or *rbohF* plants after mock and pathogen (*avrRpt2*) inoculations. The leaves were sampled 48 hours after treatments. The error bars represent SD. Asterisks denote a significant difference from mock treatment (*t* test, $P < 0.05$). The experiment was repeated two times with similar results. (**F**) SAR response in distal leaves of Col-0, *sid2*, and *gly1 gli1* plants treated locally with water or SA (500 μM). The virulent pathogen (DC3000) was inoculated 48 hours after local treatments. Error bars indicate SD ($n = 4$). Asterisks denote a significant difference from mock treatment (*t* test, $P < 0.05$). The experiment was repeated two times with similar results. (**G**) Pip levels in Col-0 and *sid2* plants after water or SA treatment. The local leaves were sampled 48 hours after treatments. The error bars represent SD. Asterisks denote a significant difference with mock (*t* test, $P < 0.05$). The experiment was repeated two times with similar results.

although ALD1-derived Pip biosynthesis from lysine does involve an additional intermediate step (*13*, *14*). Therefore, we tested whether *ALD1* overexpression could increase Pip levels by transiently overexpressing *ALD1-GFP* in *Nicotiana benthamiana* plants. As shown before (*17*), ALD1-GFP (green fluorescent protein) localized to the chloroplasts (fig. S6E), and overexpression of *ALD1* increased Pip levels by ~400-fold (fig. S6F). These data suggest that increased *ALD1* transcription results in Pip accumulation and that the intermediate steps following ALD1 activity are not rate-limiting for Pip biosynthesis.

Next, we assayed *ALD1* transcript and Pip levels in SAR-compromised mutants defective in the G3P branch of the SAR pathway. The *mgd1 dgd1* and *gly1 gli1* mutants expressed WT-like levels of *ALD1* in infected leaves but were unable to induce WT-like *ALD1* expression in the distal tissue (fig. S6D). This further correlated with their Pip levels; *mgd1 dgd1* and *gly1 gli1* plants accumulated WT-like levels of Pip in infected but not in distal tissue (Fig. 5, D and E). The ROS- and NO-defective *rboh* and *noa1 nia2* mutants, respectively, also accumulated WT-like levels of Pip in infected but not in distal tissue (Fig. 5E and fig. S6G). Together, these results suggest that de novo synthesis of Pip in the distal leaves requires the functional NO-ROS-AZA-G3P branch of the SAR pathway.

Notably, the SA biosynthetic mutant *sid2* was also compromised in distal accumulation of both Pip and ROS (fig. S7, A and B) (*18*). As expected, inoculated leaves or PEX from avirulent pathogen–infected *sid2* plants showed normal induction of G3P but not SA (fig. S7, C and D). These results suggest that in addition to G3P, avirulent pathogen–induced de novo synthesis of Pip in the distal leaves also requires SA. Consistent with a dual requirement for SA and G3P for SAR, SA treatment conferred SAR on *sid2* but not on *gly1 gli1* plants (Fig. 5F). Conversely, G3P did not confer SAR on *sid2* but was able to restore SAR in *mgd1 dgd1*, *gly1 gli1*, and *rbohD* plants (fig. S6E). Moreover, local application of SA was associated with increased accumulation of Pip (Fig. 5G). Together, these results suggest that both G3P and SA were required for de novo synthesis of Pip in the distal leaves. However, these results do not explain why treatment with Pip was unable to restore SAR in *sid2* plants (fig. S5A). To probe this question, we assayed Pip levels in distal tissues of *sid2* plants after localized application of Pip. Unlike WT, the *sid2* plants did not accumulate Pip in their distal leaves (fig. S7F). Likewise, *gly1 gli1* plants also showed impaired de novo synthesis of Pip in their distal leaves (fig. S7F). Thus, basal levels of SA and G3P are required for de novo synthesis of Pip in the distal tissues, a requirement that explains why localized application of Pip is unable to confer SAR on *sid2* plants.

DISCUSSION

The finding that seemingly unrelated chemicals (NO, ROS, AzA, G3P, SA/MeSA, Pip, DA) function as SAR inducers led to the notion that SAR signaling involves multiple independent signals. However, our work established that NO, ROS, AzA, and G3P function in a linear pathway that functions in parallel with SA-derived signaling to induce SAR. Here, we establish the relationship between Pip and the SA/G3P-derived parallel signaling pathways. We find that Pip functions upstream of the NO-ROS-AzA-G3P branch of SAR signaling and is consistent with a recent study that suggested an SA-independent function for Pip in SAR (*18*). Pip has been suggested to induce SA levels (*12*). However, we show that Pip does not increase the expression of the SA marker *PR-1*; these data are in turn consistent with our finding of basal levels of SA in Pip-treated plants. Our results suggest that Pip does not feed into the SA branch of the SAR pathway and primarily functions upstream of the NO-ROS-AzA-G3P branch of the SAR pathway. The placement of Pip in the NO-ROS-AzA-G3P branch is further supported by genetic and chemical analysis of mutants.

The Pip synthesis-deficient *ald1* mutant accumulates SA, but not ROS, AzA, or G3P, in response to infection with avirulent pathogen. Correspondingly, ROS, AzA, or G3P application induces SAR in *ald1* plants, but SA application does not. Furthermore, exogenous Pip cannot induce SAR on mutants impaired in pathogen-responsive biosynthesis/accumulation of NO (*noa1 nia2*), ROS (*rbohD/rbohF*), AzA (*mgd1 dgd1*), and G3P (*gly1 gli1*). This lack of response indicates that Pip functions upstream of ROS in the NO-ROS-AzA-G3P branch of SAR signaling. Consistent with the dual requirement for G3P- and SA-derived signaling for SAR, Pip is unable to induce SAR on mutants defective in SA biosynthesis (*sid2*). Likewise, NO and ROS, which serve downstream of Pip, are also unable to induce SAR on *sid2* (*6*).

Both SA and G3P contribute to avirulent pathogen-responsive Pip accumulation. Neither *sid2* (which contains low basal SA and is defective in pathogen-inducible SA accumulation) nor *gly1* (which is defective in pathogen-inducible G3P accumulation) mutants accumulate Pip in their distal tissue. However, this defect is not detected in the infected leaves of these mutants. One possibility is that Pip accumulation can be induced as long as threshold levels of either SA or G3P are achieved. Thus, the SA-defective *sid2* plants accumulate threshold levels of G3P (but not SA), while *gly1* plants accumulate threshold levels of SA (but not G3P) in their infected tissue, resulting in Pip accumulation. This is not the case in distal tissue, which does not accumulate nearly as much SA or G3P as infected tissue. Consistent with this notion, exogenous application of SA on *sid2* plants increases SA levels in the distal tissues as well as boosts Pip levels and is therefore able to confer SAR on *sid2* plants. On the other hand, exogenous Pip cannot confer SAR on *sid2* plants because these plants lack SA in their distal tissues, which is required for the de novo synthesis of Pip in the distal leaves. Like SA, G3P is also required for the de novo synthesis of Pip in distal tissue. Exogenous G3P was able to confer SAR on *ald1* plants, suggesting that increased levels of G3P override a requirement for Pip, as long as plants contain WT levels of SA.

Our results also establish an important role for SA in the distal tissues, a possibility that was discounted by an earlier study suggesting that SA was not the mobile signal (*19*). This work was based on grafting experiments carried out between tobacco plants expressing the salicylate hydroxylase gene *nahG* and WT tobacco. The WT scion grafted onto *nahG* rootstock was able to confer normal SAR, suggesting that SA was not a mobile signal. It is important to note that SA is primarily transported via the apoplast (*10*) and can thereby escape degradation by the cytoplasmic nahG. This possibility is in agreement with SA levels reported in the distal tissues of WT and nahG plants (*19*).

On the basis of these results, we propose that Pip functions primarily upstream of the NO-ROS-AzA-G3P branch of the SAR pathway in infected tissue (Fig. 6). The Pip-induced SAR is dependent on the biosynthesis of downstream signals, and this explains why Pip requires more time to confer effective SAR compared to downstream signals like G3P. Pathogen infection induces Pip accumulation in the infected tissue, which in turn induces the accumulation of NO, ROS, AzA, and G3P. SA and G3P are transported to the distal leaves where they induce de novo Pip biosynthesis and thereby reactivate the NO, ROS, and AzA cascade culminating in the de novo biosynthesis of G3P. Notably, the absence of Pip does not alter the biosynthesis of SAR signals that act upstream of Pip. Clarifying the importance of Pip accumulation in

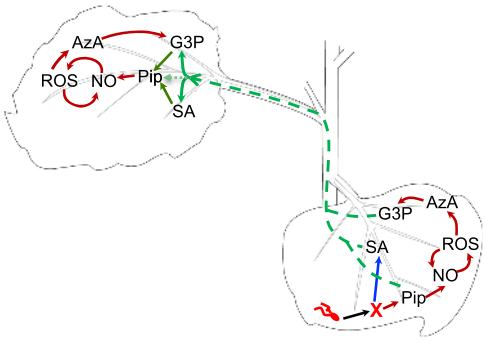

Fig. 6. A simplified model illustrating the relationship between SA, G3P, and Pip in local and distal leaves. Inoculation of avirulent pathogen triggers independent signaling events that lead to accumulation of SA and NO in the local leaves. NO triggers synthesis of ROS, which catalyze oxidation of free C18-unsaturated FAs that are released from membrane lipids (*4*). NO and ROS operate in a feedback loop. Oxidation of C18 FAs generates AzA, which triggers biosynthesis of G3P via up-regulation of genes encoding G3P biosynthetic enzymes. Of these, chemical signals SA, G3P, AzA, and Pip are detected in the PEX collected from leaves inoculated with avirulent pathogen. SA and G3P are required for synthesis of Pip in the distal leaves. Exogenous G3P, but not SA, can overcome a requirement for Pip and confer SAR on *ald1* plants that are unable to synthesize Pip. Dashed green lines indicate transport of SA, G3P, and Pip from local to distal tissues.

infected versus distal tissues and elucidating how SA and G3P regulate Pip biosynthesis will yield further insights into the relationships between these various SAR signals.

MATERIALS AND METHODS

Plant growth conditions and genetic analysis

Plants were grown in MTPS 144 Conviron walk-in chambers at 22°C, 65% relative humidity, and a photoperiod of 14 hours. These chambers were equipped with cool white fluorescent bulbs (Sylvania, FO96/841/XP/ECO). The photon flux density of the day period was 106.9 µmol m^{-2} s^{-1} (measured using a digital light meter; Phytotronics Inc.). Plants were grown on autoclaved PRO-MIX soil (Premier Horticulture Inc.). Soil was fertilized once using Scotts Peters 20-10-20 peat lite special general fertilizer that contained 8.1% ammoniacal nitrogen and 11.9% nitrate nitrogen (Scottspro.com). Plants were irrigated using deionized or tap water. The *gly1*, *gli1* (*nho1*), *mgd1*, *dgd1*, *noa1*, *noa1 nia2*, *rbohF*, and *rbohD* plants were described earlier (*4*–*6*, *15*).

NO and ROS staining and quantification

For NO staining, the adaxial side of leaves was infiltrated with 4 µM DAF-FM DA, and after 5 min of incubation in the dark, leaves were observed under an Olympus FV1000 laser-scanning confocal microscope using a 488-nm laser. NO quantification was carried out as described earlier (*6*). For ROS staining, leaves were stained with 3,3′-diaminobenzidine as described before (*20*). For H_2O_2 quantification, leaves were homogenized in 40 mM tris-HCl (pH 7.0), and to this, 20 µM 2′,7′-dichlorofluorescein was added. The samples were incubated for 1 hour in the dark, and the H_2O_2 levels were measured using a spectrofluorometer. The concentration of H_2O_2 was determined as nanograms per millligram of protein by extrapolating from the standard H_2O_2 curve.

For ESR spectra, 0.1 g of leaves was homogenized in 500 µl of 50 mM Hepes buffer (pH 6.9) containing 50 mM POBN, and 10 µl of this homogenate was loaded onto a graduated capillary tube in a flat cell. Electron paramagnetic resonance (EPR) spectra were measured at room temperature using a Bruker ESP 300 X-band spectrometer set at 5-mW microwave power, 100-kHz modulation frequency, 1-G modulation amplitude, and 9.687-GHz microware frequency. Values of ESR signals were calculated from the maximum signal-to-noise ratio of recorder traces and corrected, if necessary, by subtracting reagent blanks determined in parallel. Signal intensity was evaluated as the peak height in ESR spectra. Standard spectra for carbon-centered radicals were created by incubating POBN with xanthine (1 mM) and xanthine oxidase (0.05 U/ml) reaction mixture.

Confocal microscopy

For confocal imaging, samples were scanned on an Olympus FV1000 microscope (Olympus America). GFP and red fluorescent protein (RFP) were excited using 488- and 543-nm laser lines, respectively. Water-mounted sections of leaf tissue were examined by confocal microscopy using a water immersion PLAPO60XWLSM 2 (numerical aperture, 1.0) objective on an FV1000 point-scanning/point-detection laser-scanning confocal microscope (Olympus) equipped with lasers spanning the spectral range of 405 to 633 nm. RFP and GFP overlay images (×40 magnification) were acquired at a scan rate of 10 ms per pixel. GFP channel (488 nm) was used to analyze DAF-FM DA–stained leaves and roots. Olympus FLUOVIEW 1.5 was used to control the microscope, image acquisition, and the export of TIFF files.

G3P, SA, AzA, and Pip quantifications

G3P quantifications were carried out as described earlier (*5*). SA and SA glucoside were extracted and measured from ~0.3 g of fresh weight leaf tissue, as described before (*21*). FA and AzA extraction was carried out as described earlier (*5*). Pip quantifications were carried out using GC–mass spectrometry.

Chemical treatments

SA, H_2O_2, G3P, AzA, Pip, and NONOate treatments were carried out by using 500, 500, 100, 500 to 1000, 500 to 1000, and 300 µM solutions, respectively. SA was prepared and diluted in water. H_2O_2 was available as 30% solution and was diluted in water. NONOate stocks were prepared in dimethyl sulfoxide and diluted in water. AzA and Pip stocks were prepared in methanol and diluted in water. All dilutions were freshly prepared before performing biological experiments. G3P was dissolved and diluted in water.

RNA extraction, RNA gel blot analyses, and quantitative real-time polymerase chain reaction

Small-scale extraction of RNA from two or three leaves (per sample) was performed with the TRIzol reagent (Invitrogen), following the manufacturer's instructions. RNA gel blot analysis and synthesis of random-primed probes for *PR-1* and *PR-2* were carried out as described previously (*22*). RNA quality and concentration were determined by gel electrophoresis and determination of A_{260} (absorbance at 260 nm). Reverse transcription (RT) and first-strand complementary DNA synthesis were carried out using SuperScript II (Invitrogen). Quantitative RT–polymerase chain reaction was carried out as described before (*23*). Each sample was run in triplicate, and *ACTINII* (At3g18780) expression levels were used as internal control for normalization. Cycle threshold values were calculated by SDS 2.3 software.

Protein extraction and immunoblot analysis

Proteins were extracted in buffer containing 50 mM tris-HCl (pH 7.5), 10% glycerol, 150 mM NaCl, 10 mM $MgCl_2$, 5 mM EDTA, 5 mM

dithiothreitol, and 1× protease inhibitor cocktail (Sigma-Aldrich). Protein concentration was measured by the Bio-Rad protein assay (Bio-Rad). For Ponceau S staining, polyvinylidene difluoride membranes were incubated in Ponceau S solution [40% methanol (v/v), 15% acetic acid (v/v), and 0.25% Ponceau S]. The membranes were destained using deionized water. Proteins (~100 μg) were fractionated on a 7 to 10% SDS–polyacrylamide gel electrophoresis gel and subjected to immunoblot analysis using ∝-NOA1 antibody (*15*). Immunoblots were developed using an enhanced chemiluminescence detection kit (Roche) or alkaline phosphatase–based color detection.

Pathogen infection and collection of phloem exudate

Inoculations with *P. syringae* DC 3000 were conducted as described before (*24*). The bacterial cultures were grown overnight in King's B medium containing rifampicin and/or kanamycin. For analysis of SAR, the primary leaves were inoculated with $MgCl_2$ or the avr bacteria (10^6 CFU ml^{-1}) and, 24 hours later, the systemic leaves were inoculated with virulent (vir) bacteria (10^5 CFU ml^{-1}). Unless noted otherwise, samples from the systemic leaves were harvested at 3 dpi. PEXs were collected as described earlier (*5*, *6*). PEX was assayed for bacterial growth to ensure that it did not contain any viable bacteria.

Conductivity assays

Electrolyte leakage was measured in 4-week-old plants. Leaves were infiltrated with $MgCl_2$ or *Pst avRpt2* (10^6 CFU/ml). After inoculation, ~5 leaf discs per plant (7 mm) were removed with a cork borer, floated in distilled water for ~30 min, and subsequently transferred to tubes containing 5 ml of distilled water. Conductivity of the solution was determined with a National Institute of Standards and Technology (NIST) traceable digital conductivity meter (Fisher Scientific) at the indicated time points. SD was calculated from four replicate measurements per genotype per experiment.

FA analysis

FA extraction was carried out by placing leaf tissue in 2 ml of 3% H_2SO_4 in methanol. After 30 min of incubation at 80°C, 1 ml of hexane with 0.001% butylated hydroxytoluene was added. The hexane phase was then transferred to vials for GC analysis. One-microliter samples were analyzed by GC on a Varian FAME 0.25-mm × 50-m column and quantified with flame ionization detection. For quantification of FAs, leaves (50 mg) were extracted together with an internal standard 17:0 (Sigma-Aldrich), and the FA levels were calculated on the basis of the detected peak areas corresponding to the FA retention time relative to the areas of the internal standard.

Galactolipid analysis

TLC analysis of galactolipids of MGDG and DGDG was carried out as described before (*25*). For MGDG and DGDG quantification, ~300 mg of *Arabidopsis* leaf tissue was suspended in 600 μl of chloroform/methanol/formic acid (20:10:1, v/v), vortexed vigorously for 5 min followed by addition of 300 μl of 0.2 M H_3PO_4, and the samples were revortexed for an additional 1 min. After a brief centrifugation for 1 min at 12,000 rpm, the lower phase was re-extracted with 300 μl of chloroform and dried under a stream of nitrogen gas. The samples were reconstituted in 1 ml of chloroform, and 100 μl was loaded on a TLC plate prepared as described earlier (*25*). The MGDG and DGDG bands were visualized under long-range ultraviolet light after spraying the TLC plate with 0.005% primulin prepared in 80% acetone. The bands were scraped and added to a glass test tube containing 20 μg of triheptadecanoin in 100 μl of chloroform/methanol (2:1, v/v). To this, 500 μl of 4.8% sodium methoxide was added, and the samples were shaken for 40 min at 150 rpm. The samples were mixed with 1 ml of hexane/MTBE (96:4, v/v) and 600 μl of 0.9% KCl, centrifuged at 500 rpm for 1 min followed by the transfer of the upper layer to a gas chromatography (GC) vial. The samples were dried, resuspended in 400 μl of hexane, and analyzed by GC on a Varian VF-17ms column (VF-17; 0.25 mm × 50 m).

Pip transport assays

For Pip transport, ^{14}C-Pip (1 μCi/ml; specific activity, 38 mCi/mmol; ViTrax Inc.) was suspended in 10 mM $MgCl_2$ and used for infiltrations with or without *avrRpt2*. The resulting solution contained 26 μM Pip and was injected into the abaxial surface of 4-week-old *Arabidopsis* leaves. Three leaves per plant were infiltrated with ~0.05 ml of ^{14}C-Pip solution. The untreated leaves were individually covered with Saran wrap to avoid any spillover. The plants were then kept in a growth chamber set at 14-hour light and 10-hour dark photoperiods. The leaf samples were extracted using the extraction method described above. The samples were quantified using a liquid scintillation counter, and extracts containing [^{14}C] radioactivity were loaded onto silica gel 60 and run using butanol/acetic acid/water (3:1:1, v/v). The TLC plates were exposed in a storage phosphorimage screen (GE), and the bands were visualized by a Typhoon PhosphorImager.

PAT-seq library preparation and data analysis

For gene expression profiling, plants were treated with 0.01% methanol or 1 mM Pip, and the samples were harvested 24 hours after treatments. RNA was isolated from three independent biological samples for each line, extracted using the TRIzol reagent, and purified using RNA columns. Poly(A) tags (PATs) were generated using 1 μg of total RNA using method B1 as described by Ma *et al.* (*26*). The resulting PATs were sequenced on an Illumina high-throughput DNA sequencing platform. The sequencing data (2.2 to 3.1 million reads per sample) were processed using the pipeline detailed by Bell *et al.* (*27*). Using the CLC Genomics Workbench suite of tools, the initial sequences obtained were demultiplexed and trimmed to remove the oligo-dT tracts and sequencing adapters. The processed tags (average length, 67 base pairs) were then mapped to the *Arabidopsis* reference genome (TAIR10). The mapping output was saved in BAM file format and used with Bedtools to determine the total count of PATs that mapped to individual annotated genes. This information was used to determine gene expression using the CLC Genomics Workbench, and statistical analysis was based on the exact test of empirical analysis of digital gene expression algorithm in the CLC Genomics Workbench. The statistical analysis is based on the "Exact Test" for two-group comparisons to calculate the *P* value, considering that the count data follow a negative binomial distribution. Genes with a total filter cutoff of twofold change and *P* values <0.05 were selected as statistically significant.

SUPPLEMENTARY MATERIALS

Supplementary material for this article is available at http://advances.sciencemag.org/cgi/content/full/4/5/eaar4509/DC1

fig. S1. The *ald1* plants accumulate basal levels of Pip.

fig. S2. Pip-induced NO is dependent on ALD1.

fig. S3. Pip-induced ROS is dependent on ALD1 and RBOHD.

fig. S4. The *ald1* plants show reduced ion leakage.
fig. S5. Pip is unable to confer SAR on mutants impaired in the SA pathway.
fig. S6. Induction of Pip is associated with *ALD1* transcript levels.
fig. S7. Induction of Pip in the distal tissues is associated with transport of SA and G3P.
table S1. Gene expression analysis in response to methanol (0.001%) and Pip treatments in *Arabidopsis thaliana*.

REFERENCES AND NOTES

1. J. D. G. Jones, J. L. Dangl, The plant immune system. *Nature* **444**, 323–329 (2006).
2. T. Gaffney, L. Friedrich, B. Vernooij, D. Negrotto, G. Nye, S. Uknes, E. Ward, H. Kessmann, J. Ryals, Requirement of salicylic acid for the induction of systemic acquired resistance. *Science* **261**, 754–756 (1993).
3. H. W. Jung, T. J. Tschaplinski, L. Wang, J. Glazebrook, J. T. Greenberg, Priming in systemic plant immunity. *Science* **324**, 89–91 (2009).
4. K. Yu, J. M. Soares, M. K. Mandal, C. Wang, B. Chanda, A. N. Gifford, J. S. Fowler, D. A. Navarre, A. Kachroo, P. Kachroo, A feedback regulatory loop between G3P and lipid transfer proteins DIR1 and AZI1 mediates azelaic-acid-induced systemic immunity. *Cell Rep.* **3**, 1266–1278 (2013).
5. B. Chanda, Y. Xia, M. K. Mandal, K. Yu, K.-T. Sekine, Q.-m. Gao, D. Selote, Y. Hu, A. Stromberg, D. Navarre, A. Kachroo, P. Kachroo, Glycerol-3-phosphate is a critical mobile inducer of systemic immunity in plants. *Nat. Genet.* **43**, 421–427 (2011).
6. C. Wang, M. El-Shetehy, M. B. Shine, K. Yu, D. Navarre, D. Wendehenne, A. Kachroo, P. Kachroo, Free radicals mediate systemic acquired resistance. *Cell Rep.* **7**, 348–355 (2014).
7. D. Wendehenne, Q.-m. Gao, A. Kachroo, P. Kachroo, Free radical-mediated systemic immunity in plants. *Curr. Opin. Plant Biol.* **20**, 127–134 (2014).
8. P. Kachroo, G.-H. Lim, A. Kachroo, Nitric oxide-mediated chemical signaling during systemic acquired resistance, in *Advances in Botanical Research*, D. Wendehenne, Ed. (Academic Press, 2015), vol. 77.
9. Q.-m. Gao, K. Yu, Y. Xia, M. B. Shine, C. Wang, D. Navarre, A. Kachroo, P. Kachroo, Mono- and digalactosyldiacylglycerol lipids function nonredundantly to regulate systemic acquired resistance in plants. *Cell Rep.* **9**, 1681–1691 (2014).
10. G.-H. Lim, M. B. Shine, L. de Lorenzo, K. Yu, W. Cui, D. Navarre, A. G. Hunt, J.-Y. Lee, A. Kachroo, P. Kachroo, Plasmodesmata localizing proteins regulate transport and signaling during systemic acquired immunity in plants. *Cell Host Microbe* **19**, 541–549 (2016).
11. B. Chanda, S. C. Venugopal, S. Kulshrestha, D. A. Navarre, B. Downie, L. Vaillancourt, A. Kachroo, P. Kachroo, Glycerol-3-phosphate levels are associated with basal resistance to the hemibiotrophic fungus *Colletotrichum higginsianum* in *Arabidopsis*. *Plant Physiol.* **147**, 2017–2029 (2008).
12. H. Návarová, F. Bernsdorff, A.-C. Döring, J. Zeier, Pipecolic acid, an endogenous mediator of defense amplification and priming, is a critical regulator of inducible plant immunity. *Plant Cell* **24**, 5123–5141 (2012).
13. P. Ding, D. Rekhter, Y. Ding, K. Feussner, L. Busta, S. Haroth, S. Xu, X. Li, R. Jetter, I. Feussner, Y. Zhang, Characterization of a pipecolic acid biosynthesis pathway required for systemic acquired resistance. *Plant Cell* **28**, 2603–2615 (2016).
14. M. Hartmann, D. Kim, F. Bernsdorff, Z. Ajami-Rashidi, N. Scholten, S. Schreiber, T. Zeier, S. Schuck, V. Reichel-Deland, J. Zeier, Biochemical principles and functional aspects of pipecolic acid biosynthesis in plant immunity. *Plant Physiol.* **174**, 124–153 (2017).
15. M. K. Mandal, A. C. Chandra-Shekara, R.-D. Jeong, K. Yu, S. Zhu, B. Chanda, D. Navarre, A. Kachroo, P. Kachroo, Oleic acid–dependent modulation of NITRIC OXIDE ASSOCIATED1 protein levels regulates nitric oxide–mediated defense signaling in *Arabidopsis*. *Plant Cell* **24**, 1654–1674 (2012).
16. M. A. Torres, J. L. Dangl, J. D. G. Jones, *Arabidopsis* gp91^{phox} homologues *AtrbohD* and *AtrbohF* are required for accumulation of reactive oxygen intermediates in the plant defense response. *Proc. Natl. Acad. Sci. U.S.A.* **99**, 517–522 (2002).
17. N. M. Cecchini, H. W. Jung, N. L. Engle, T. J. Tschaplinski, J. T. Greenberg, ALD1 regulates basal immune components and early inducible defense responses in *Arabidopsis*. *Mol. Plant Microbe Interact.* **28**, 455–466 (2015).
18. F. Bernsdorff, A.-C. Döring, K. Gruner, S. Schuck, A. Bräutigam, J. Zeier, Pipecolic acid orchestrates plant systemic acquired resistance and defense priming via salicylic acid-dependent and -independent pathways. *Plant Cell* **28**, 102–129 (2016).
19. B. Vernooij, L. Friedrich, A. Morse, R. Reist, R. Kolditz-Jawhar, E. Ward, S. Uknes, H. Kessmann, J. Ryals, Salicylic acid is not the translocated signal responsible for inducing systemic acquired resistance but is required in signal transduction. *Plant Cell* **6**, 959–965 (1994).
20. A. Daudi, J. A. O'Brien, Detection of hydrogen peroxide by DAB staining in *Arabidopsis* leaves. *Bio-Protoc.* **2**, e263 (2012).
21. A. C. Chandra-Shekara, M. Gupte, D. Navarre, S. Raina, R. Raina, D. Klessig, P. Kachroo, Light-dependent hypersensitive response and resistance signaling against Turnip Crinkle Virus in *Arabidopsis*. *Plant J.* **45**, 320–334 (2006).
22. A. Kachroo, S. C. Venugopal, L. Lapchyk, D. Falcone, D. Hildebrand, P. Kachroo, Oleic acid levels regulated by glycerolipid metabolism modulate defense gene expression in *Arabidopsis*. *Proc. Natl. Acad. Sci. U.S.A.* **101**, 5152–5157 (2004).
23. D.-X. Zhang, P. Nagabhyru, C. L. Schardl, Regulation of a chemical defense against herbivory produced by symbiotic fungi in grass plants. *Plant Physiol.* **150**, 1072–1082 (2009).
24. Y. Xia, Q.-M. Gao, K. Yu, L. Lapchyk, D. Navarre, D. Hildebrand, A. Kachroo, P. Kachroo, An intact cuticle in distal tissues is essential for the induction of systemic acquired resistance in plants. *Cell Host Microbe* **5**, 151–165 (2009).
25. Z. Wang, C. Benning, *Arabidopsis thaliana* polar glycerolipid profiling by thin layer chromatography (TLC) coupled with gas-liquid chromatography (GLC). *J. Vis. Exp.* **49**, e2518 (2011).
26. L. Ma, P. K. Pati, M. Liu, Q. Q. Li, A. G. Hunt, High throughput characterizations of poly(A) site choice in plants. *Methods* **67**, 74–83 (2014).
27. S. A. Bell, C. Shen, A. Brown, A. G. Hunt, Experimental genome-wide determination of RNA polyadenylation in *Chlamydomonas reinhardtii*. *PLOS ONE* **11**, e0146107 (2016).

Acknowledgments: We thank W. Havens, L. Lapchyk, and A. Crume for technical support and J. Johnson for help with biochemical profiling. We also thank J. Greenberg and J. Zeier for useful discussions, M. A. Torres and J. Dangl for *rbohD* and *rbohF* seeds, and Arabidopsis Biological Resource Center for *ald1* seeds. **Funding:** This work was supported by grants from the NSF (MCB#0421914, #1243849, and IOS#051909), the Kentucky Science and Engineering Foundation (#1244), the Kentucky Soybean Board (3084113467), and the Kentucky Tobacco Research and Development Center. **Author contributions:** The SAR experiments, metabolite levels, gene expression, and protein levels were analyzed by C.W., R.L., G.-H.L., and K.Z. RNA sequencing analysis was carried out by L.d.L., G.-H.L., and A.G.H. K.Y. developed the Pip quantification procedure. K.Y. and G.-H.L. generated double mutant plants. Galactolipid and FA analysis were carried out by G.-H.L. and K.Y. Transient expression assays were carried out by G.-H.L. and C.W. P.K. conceptualized the research. P.K. and A.K. supervised the project and wrote the manuscript with help from all the authors. **Competing interests:** The authors declare that they have no competing interests. **Data and materials availability:** All data needed to evaluate the conclusions in the paper are present in the paper and/or the Supplementary Materials. Additional data related to this paper may be requested from the authors.

Submitted 1 February 2018
Accepted 19 April 2018
Published 30 May 2018
10.1126/sciadv.aar4509

Citation: C. Wang, R. Liu, G.-H. Lim, L. de Lorenzo, K. Yu, K. Zhang, A. G. Hunt, A. Kachroo, P. Kachroo, Pipecolic acid confers systemic immunity by regulating free radicals. *Sci. Adv.* **4**, eaar4509 (2018).

ScienceAdvances

Pipecolic acid confers systemic immunity by regulating free radicals

Caixia Wang, Ruiying Liu, Gah-Hyun Lim, Laura de Lorenzo, Keshun Yu, Kai Zhang, Arthur G. Hunt, Aardra Kachroo and Pradeep Kachroo

Sci Adv **4** (5), eaar4509.
DOI: 10.1126/sciadv.aar4509